PHYSICAL REVIEW B **80**, 085306 (2009)

Phase diagram of Sr on Si(001): A first-principles study

Kevin Garrity*
Department of Physics, Yale University, New Haven, Connecticut 06520-8120, USA

Sohrab Ismail-Beigi
Department of Applied Physics and Department of Physics, Yale University, New Haven, Connecticut 06520-8120, USA

(Received 5 February 2009; revised manuscript received 11 June 2009; published 11 August 2009)

The best known method for growing epitaxial oxides on silicon requires the deposition of 1/2 monolayer of an alkaline earth metal, usually Sr, as the first step; however, the details of this process are not well understood. Using first-principles density functional theory calculations, we compute the total energies and vibrational free energies of several classes of Sr on Si(001) structures. These structures, in particular those with submonolayer Si reconstructions, allow us to explain the observed phase diagram of submonolayer Sr on Si(001). We analyze the electronic states of key structures using maximally localized Wannier functions and present simulated scanning tunneling microscopy images of key structures and find that they compare well with recent experiments. Our results clarify the role of temperature in epitaxial oxide growth on silicon, predict an experimentally verified low temperature path to epitaxy, and may be important in finding pathways to epitaxy between silicon and other oxides.

DOI: 10.1103/PhysRevB.80.085306 PACS number(s): 68.47.Fg, 71.15.Mb, 81.15.Hi

I. INTRODUCTION

The integration of new materials with current microelectronic technology is an important prerequisite for both improving many current technologies as well as creating new ones. In particular, the growth of epitaxial oxides on silicon is a key goal for the continuation of Moore's law in current complementary metal-oxide semiconductor transistors as well as a necessary component for many proposed devices.

As the electronic industry strives to pack higher densities of faster transistors onto a silicon wafer, the area of all the transistors must decrease. Despite this scaling, due to limitations on the charge and voltage, the capacitance across the dielectric layer of a transistor must remain constant.[1] In the past, the solution to this problem has been to decrease the thickness of the dielectric layer, currently made primarily of silicon dioxide, in order to maintain the desired capacitance per unit area. Unfortunately, current dielectric layers are only a few atomic layers thick and further decreases in the thickness of this layer will result in unacceptably large quantum mechanical tunneling (leakage) currents through the dielectric.[1]

One solution is to replace the silicon dioxide dielectric with a material which has a higher dielectric constant, thus allowing the dielectric layer to be physically thicker but still have the desired capacitance.[2,3] In order for this approach to be successful, the new material must have a high quality interface with silicon which minimizes the scattering of electrons in the channel region of the transistor. Complex transition metal oxides deposited epitaxially on Si are one class of materials which can fulfill both requirements.

Beyond current technological concerns, the epitaxial integration of complex oxides with silicon would also allow the many interesting and potentially useful properties of oxides to be used in new devices, including but not limited to ferroelectricity, ferromagnetism, multiferroic behavior, and high-T_c superconductivity. In principle, these properties could be used in memory applications, improved transistors, or other novel spin-based devices; however, integrating these properties into practical devices will require atomic level control over oxide interfaces with silicon.

Currently, all examples of oxides grown epitaxially on silicon have required the deposition of a submonolayer template layer of Sr, Ba, or Ca on the silicon as a first step.[4,5] During this initial deposition, experiments with *in situ* sample characterization observe several different surface reconstructions. However, the role of these reconstructions in preparing the surface as an oxide growth template which forms the eventual interface[6] with the complex oxide is unknown. Here, we propose several submonolayer Sr on Si(001) structures which explain these reconstructions and which enable us to clarify the role of temperature plays in creating an effective oxide template. Our knowledge of Sr on Si(001) has allowed us to predict an experimentally verified low temperature path to oxide epitaxy.[7]

In addition to understanding this particular oxide growth method, we hope that, over longer time scales, the knowledge acquired by studying Sr on Si will help explain the failure of other elements to provide an effective template layer for oxide growth. La, in particular, would be very intriguing as an oxide template due to the high dielectric constant and large band offsets of $LaAlO_3$ with Si. Unfortunately, La has thus far failed as a template layer for epitaxial growth on Si.[8]

This paper is organized as follows. In Sec. II we describe our calculational methods. In Sec. III we present a review of experimental work on Sr on Si(001). In Sec. IV we present results for Sr deposited on a standard dimerized surface: these findings are largely in agreement with previous theoretical work[9] but fail to explain many of the experimental results. In Sec. V we present results for Sr on modified dimer surfaces which allow us to rule out this entire class of structures. In Sec VI, we present results for Sr on submonolayer silicon surfaces. In Sec. VII we use the results of Secs.

IV–VI to explain the experimental data and present a phase diagram for submonolayer Sr on Si(001). In Sec. VIII we present computed scanning tunneling microscopy (STM) images for the most stable 1/6 monolayer (ML) structure which also turn out to compare well with experimental findings. Finally, in Sec. IX, we present our conclusions.

II. METHODS

A. Total energies

Our calculations were based on first-principles density functional theory (DFT) calculations using a plane-wave basis set.[10,11] We used the Perdew-Burke-Ernzerhof generalized gradient approximation[12] (PBE GGA) to approximate the exchange correlation functional. In order to minimize the number of electrons in our calculations, we employed norm-conserving Troullier-Martins pseudopotentials[13] to simulate the valence electrons. For silicon, we used $3s$, $3p$, and $3d$ projectors (d local) with cutoff radii of $r_s=r_p=r_d=2.25$ bohr and the reference atomic configuration $3s^2 3p^2 3d^0$. For Sr, we treated the semicore $4s$ and $4p$ states as valence electrons in addition to the valence $3d$, $5s$, and $5p$ states ($3d$ local) with cutoff radii of $r_s=1.3$ bohr, $r_p=r_d=2.0$ bohr and reference configuration $5s^1 4d^1 5p^0$. The semicore states are necessary to properly describe the physics of Sr. With semicore states, our calculated Sr lattice constant was 6.05 Å, in excellent agreement with experiment, but when we did not include semicore states in our Sr pseudopotentials, we found poor transferability between different atomic states and a lattice constant that varies 5% depending on apparently irrelevant numerical choices for our reference configuration or cutoff radii.

All our calculations were run at the theoretical lattice constant of silicon, which we calculated to be 5.456 Å and with a plane-wave cutoff energy of 60 Ry. We used a slab geometry with periodic boundary conditions in the x and y directions and a finite thickness in the z direction, which is the (001) direction in the Si crystal. This geometry creates two surfaces, one on each side of the slab. We treated the surfaces symmetrically by adding Sr to both sides to create two physically identical surfaces (see the next paragraph for why this is important). The slab was simulated with at least eight layers of silicon plus an equivalent of eight silicon layers of vacuum. We found binding energies to be converged to within 0.01 eV/Sr using a 6×6 k-point sampling per 1×1 surface unit cell of silicon with a Fermi-Dirac smearing temperature of 0.1 eV. In this work, the z direction is the surface normal, x is by default the direction in which a clean Si(001) surface doubles it periodicity by dimerizing, and y is orthogonal to both x and z.

Initially, we attempted to decrease the size of our calculation by only using one Sr on Si surface and passivating the opposite slab surface with hydrogen, as per Ashman *et al.*[9] and Stekolnikov *et al.*[14] among others. However, we found that these configurations were insufficient to converge binding energies to within 0.01 eV/Sr. Table I compares the results of several different methods of approximating a Si slab to our eight layer symmetric surface method. The reason for the insufficiency is the following: an examination of the electric potentials of the asymmetric calculations revealed significant long range electric fields through the vacuum. Due to the different charge densities at the two surfaces, this electric field is unavoidable, and the energy associated with it seems sufficient to change the computed total energy in an uncontrolled fashion.

TABLE I. Comparison of Sr binding energies for different Si slab configurations. All energies are relative to the eight layer symmetric configuration used in this work which has the same atomic configuration on both sides of the slab. For the unreconstructed configurations, each Si in the bottom layer is frozen to its bulk position and two H atoms per surface Si are used to passivate its dangling bonds. In the reconstructed configurations, the bottom of the slab is dimerized with one H atom per surface Si.

Sr coverage (ML)	Slab configuration	ΔE_{bind} (eV)
1/4	4 layers unreconstructed	−0.33
1/4	4 layers reconstructed	0.10
1/4	8 layers reconstructed	−0.04
1/4	8 layers symmetric	≡0.00
1/2	4 layers unreconstructed	−0.22
1/2	4 layers reconstructed	0.13
1/2	8 layers reconstructed	−0.02
1/2	8 layers symmetric	≡0.00
1/2	12 layers symmetric	0.01

Sr binding energies were calculated relative to a bare silicon surface in the $p(2\times2)$ configuration and an isolated Sr atom at rest in vacuum. More positive binding energies mean stronger binding. In this work, we considered many surfaces with nonstoichiometric Si coverages, i.e., less than a full ML of Si on the surface, which required the use of a bulk Si reservoir to calculate binding energies. The chemical potential of the bulk reservoir was determined by subtracting the two nearest full monolayer silicon slab calculations and dividing the difference by the number of silicon atoms. For example, to determine the binding energy of a structure with eight full layers of Si plus two extra Si atoms per side, we used a chemical potential determined from the eight and ten layer Si slab calculations. This method was used to approximate the energy of bulk Si to the same accuracy as the rest of the slab and to remove an ambiguity as to whether a structure with a partial Si layer should be considered as adding bulk atoms to a thinner reference slab or subtracting bulk atoms from a thicker reference slab. For a sufficiently thick reference slab, this method for determining the chemical potential will give the same result as the more intuitive method of using an *ab initio* bulk Si calculation to determine the chemical potential, but our method converges faster for finite-sized slabs.

B. Phonon free energies

Most first-principles calculations assume that contributions to the free energy from the vibrational degrees of freedom of similar structures are either too small or too similar

to be relevant at experimental temperatures. However, since we were examining temperature dependent effects and small energy differences, we were forced to consider phonon contributions to the free energies. Phonon calculations require the first derivative of the charge density with respect to the nuclear positions, which we calculated using DFT perturbation theory.[15–17]

Our method for calculating the free energy of large slabs with periodic boundary conditions in the x and y directions depended on the locality of the dynamical matrix in real space. First, we calculated the dynamical matrix on a coarse grid in (k_x,k_y) space. Next, we Fourier transformed to get the dynamical matrix in (x,y) space and we checked to see if the matrix elements between atoms which were well separated in real space had decayed to negligible values. Once we had the real-space dynamical matrix with sufficient range such that any further matrix elements would be negligible, we could Fourier transform back to (k_x,k_y) space exactly and therefore calculate the dynamical matrix at any k point essentially exactly. We found that real-space matrix elements typically converged within three 1×1 unit cells of silicon. In order to ensure the convergence of low frequency modes in a computationally efficient manner (see discussion by Mounet and Marzari[18]), we enforced the translational acoustic sum rule by editing the diagonal elements of the real-space dynamical matrix D,

$$D_{ij}^{\alpha\alpha} = -\sum_{\beta\neq\alpha} D_{ij}^{\alpha\beta}, \tag{1}$$

where α and β label the atoms in the system and i and j label the x, y, or z direction. Enforcing the acoustic sum rule ensures that moving all the atoms collectively results in exactly zero restoring force and therefore that the frequencies of the three acoustic modes do in fact go to zero at Γ.

Once we had the real-space dynamical matrix, we used the above method to sample the phonon dispersion for a dense k-point grid sufficient to converge the free energy. The free energy was calculated with the standard formula for quantum harmonic oscillators,

$$F = E_0 + \sum_i \frac{1}{2}\hbar\omega_i + \ln[1-\exp(-\hbar\omega_i/k_BT)], \tag{2}$$

where E_0 is the total ground state energy of the system as determined by the plane-wave calculation, ω_i are the phonon frequencies, k_B is Boltzmann's constant, and T is the absolute temperature. For a slab system, the sum over i represents both the sums over both the $3N_{atoms}$ modes in the unit cell as well as (k_x,k_y) space.

While the Sr atoms on the surface only interacted significantly with the first three to four layers of Si directly, we still needed to converge our free energies with respect to the thickness of our slab in order to properly capture the differences between low frequency modes in the z direction. In order to accomplish this in a computationally efficient manner, we attached additional layers of bulk Si to the *ab initio* slab and converged free energy differences as a function of the number of added bulk layers (see Fig. 1). Specifically, we first derived an accurate *ab initio* second-nearest-neighbor model for the dynamical matrix of bulk Si. Second, we computed the *ab initio* dynamical matrix elements of all atoms comprising the surface and first four layers of Si of the slab. Third, to connect these slab data to the added bulk Si layers, we replaced the dynamical matrix elements connecting the third and fourth Si slab layers to the added bulk by those appropriate to the bulk second-nearest-neighbor model. The free energy differences are converged to 1 meV after attaching ten layers of bulk silicon to four layers of slab data as shown in Fig. 1.

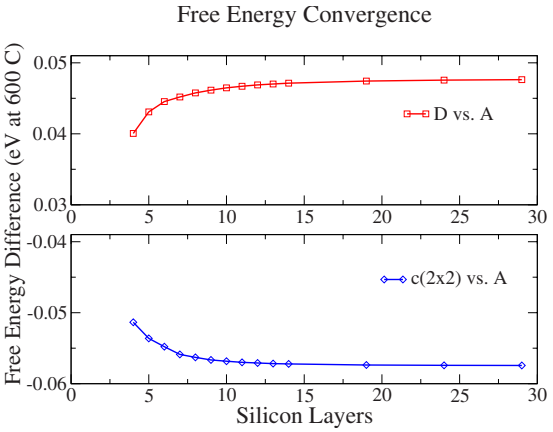

FIG. 1. (Color online) Convergence data for vibrational free energies versus number of bulk silicon layers added to the slab for 1/2 ML structures (see Figs. 2 and 6 for all the A and all D structures and Fig. 7 for the $c(2\times2)$ structure). Top: vibrational free energy of all A structure minus all D structure. Bottom: vibrational free energy of all A structure minus $c(2\times2)$ structure. We found that convergence to 1 meV/Sr at 600 °C is achieved after ten layers of Si were added to a four layer *ab initio* calculation.

C. Energy barriers

Other potential sources of temperature effects are kinetic barriers which prevent the system from reaching true thermodynamic equilibrium. In order to estimate these kinetic effects for key configurations, we performed energy barrier calculations for typical atomic motions. Energy barriers (E_{bar}) were determined using the nudged elastic band method plus climbing images, which determines the energy of the transition state between two local minima.[19,20] We then used simple transition state theory to estimate transition rates,

$$R = \nu\exp(-E_{bar}/kT). \tag{3}$$

The exponential prefactor (ν) was estimated from our phonon calculations. We expect these rates to give a good order of magnitude estimate for the rate limiting steps which dominate the motion of surface atoms.

D. Wannier functions

Finally, maximally localized Wannier function calculations were performed in order to analyze electronic structure and surface chemistry.[21] We considered several different Wannier function schemes to analyze the surface bonding. To

get a qualitative understanding of our surfaces, we used a basis consisting of Sr *s* and *d* orbitals plus sp^3-like dangling bonds on surface silicon atoms. In order to get a more quantitative understanding of the surface, we also considered a full sp^3 basis for the silicon. Using the full sp^3 basis allowed us to create an exact first-principles tight-binding model of the surface near the Fermi level, but the additional Wannier functions did not change our qualitative interpretation of the surface bonding. All of the densities of states plots in this work were obtained by projecting onto Wannier states. The advantage of projecting onto Wannier functions rather than the more commonly used atomic orbitals is that Wannier functions are orthonormal, maximally localized, and complete within the chosen Hilbert space, which we generally set to be a few eV around the Fermi level.

III. REVIEW OF EXPERIMENTAL WORK

The first step of the only known pathway to epitaxial oxide growth on Si(001) is to deposit submonolayer coverages of an alkaline earth metal on silicon near 600 °C. The first structures of this type used Sr,[4] but the method has been expanded to Ba and Ca.[5] Experiments indicate that Sr coverages between 1/4 and 1/2 ML are suitable for oxide growth,[22] but the role of high temperature Sr deposition in promoting epitaxial growth is unclear.

Previous high temperature reflection high-energy electron diffraction (RHEED),[4,22] low-energy electron diffraction,[23] and STM[24,25] studies of the surface found that the surface evolves from the 2× reconstruction exhibited by the bare silicon surface to a 3× structure at 1/6 ML, which is then replaced by a 2× structure at 1/4 ML. The final 2× structure is observed to be stable up to 1/2 ML Sr coverage. These shifting diffraction patterns are often used for calibration in oxide growth procedures. Unfortunately, their origin has up to now been largely unknown.

Diffraction experiments on the silicon surface typically suffer from the fact that the standard Si(001) surface displays terraces separated by single height steps with reconstructions rotated by 90°, resulting in diffraction data which contain a mixture of the two terminations. This mixture of surface termination prevents a clear determination of the relative alignments of the observed reconstructions. New data from the experiments of our collaborators, Reiner *et al.*,[7] avoided this issue by using specially prepared silicon wafers. They deposited Sr on a 4° miscut silicon wafer using molecular beam epitaxy and analyzed the surface using RHEED. The large miscut angle decreases the size of the silicon terraces, which both reduces the influence of strain effects and increases the influence of step energies.[26] The combination of these two effects causes all of the silicon dimer rows to align on all terraces, removing an ambiguity in the interpretation of RHEED results.

These new RHEED data showed an unexplained temperature dependence (see Table II). At low temperatures (25 °C), the experiments indicated that from 0 ML up to 1/2 ML of Sr coverage, the surface retains the 2×1 symmetry of the initial dimerized silicon surface. However, at high temperatures (600 °C), more complicated phases emerged. The surfaces started with 2×1 symmetry at 0 ML but transitioned to a 2×3 pattern at 1/6 ML. As the Sr coverage was further increased, at around 1/4 ML the pattern again changed to a 1×2 pattern, which continued until 1/2 ML. These high temperature measurements cannot be explained by existing theory work of Sr on Si(001), as we explain below.

TABLE II. Experimental symmetry patterns observed with RHEED on miscut silicon wafers (Ref. 7).

Sr coverage (ML)	$T=25$ °C	$T=600$ °C
0	2×1	2×1
1/6	Disordered 2×1	2×3
1/2	2×1	1×2

IV. STANDARD DIMERIZED SURFACES

To orient the reader, we first summarize key facts concerning the bare Si(001) surface (see Ref. 27 and references therein). The atoms of the top layer of the unreconstructed Si(001) surface are each missing two covalent bonds. The surface has a first-order reconstruction whereby each surface Si atom pairs with a neighbor and forms a strong dimer bond. Due to the highly directional sp^3 bonding with the second-layer Si atoms, all of the dimers are forced to lie in the same direction, perpendicular to the bonds between the first and second-layer atoms. These dimers prefer to arrange themselves into rows, which minimizes bond stretching. This symmetry breaking dimerization causes the periodicity of the surface to double in the *x* direction, leading to a 2×1 reconstruction. After dimerization, each surface atom still has one half-filled dangling bond. In order to further reduce the energy of the surface, each dimer has a further and weaker symmetry breaking reconstruction: each dimer buckles in the *z* direction, creating an upper atom and a lower atom (see Fig. 2). This reconstruction pushes the upper atom toward a more bulklike sp^3 geometry with a lower energy dangling sp^3-like orbital, and it pushes the lower atom into a more planar sp^2 geometry with a higher energy p_z-like dangling orbital. Then one electron is transferred from the dangling orbital of the lower atom to the upper atom, partially opening a surface band gap. Furthermore, the dimers alternate buckling direction going down each row. Despite these reconstructions, the silicon surface still features one unpassivated dangling orbital per surface silicon and tends to accept electrons.

In our first attempt to understand low coverages of Sr on the surface, we assumed that the silicon remains in its canonical dimer row pattern and that the Sr simply sits "on top" of this silicon surface. We calculated the binding energies of several different structures and found the results to be in agreement with Ashman *et al.*[9] In general, we found the binding energy per Sr to be at least 3.5 eV/Sr at coverages of up to 1/2 ML (a more positive binding energy indicates strong binding). This shows that almost all of the deposited Sr will remain on the surface for typical deposition tempera-

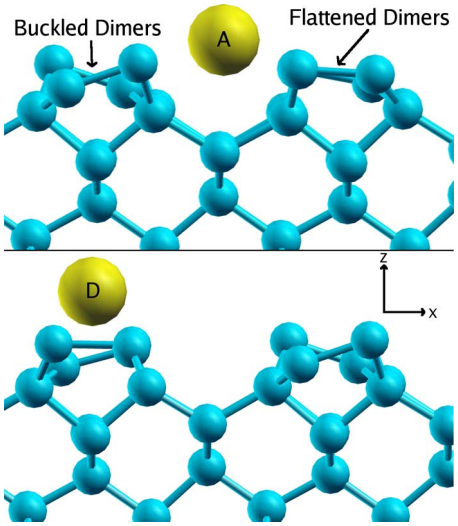

FIG. 2. (Color online) Side view of A site (top) and D site (bottom) isolated Sr. Both figures feature both flattened and buckled dimers. The single large (gold) sphere in each figure is the Sr adatom, while the Si atoms are the smaller (blue) spheres.

tures of 600 °C. In fact, at 600 °C and 1/2 ML coverage, the pressure of an ideal gas of Sr above the surface would be 9×10^{-12} Pa, well below typical experimental pressures of $\sim10^{-8}$ Pa.

To begin our search for submonolayer Sr surface structures, we compared possible binding sites for Sr adatoms. We found that isolated Sr atoms have two local minima on the silicon surface, which we called site A and site D in accordance with Ashman *et al.*[9] (see Fig. 2 and Table III). We found that site A is most stable, with a binding energy of 3.64 eV. Site D was 0.41 eV less stable; therefore, we expect all the Sr atoms to occupy A sites at low coverages. For both the A and D sites, one of the silicon dimers next to the Sr atom becomes flattened and elongated. This effect has been attributed to the Sr donating two electrons to the dangling bonds on the silicon surface, which causes both dangling bonds on the dimer to become filled.[9] When both dangling bonds are filled, the charge transfer mechanism which is responsible for stabilizing the Si buckling reconstruction (summarized above) is eliminated, which causes the dimer to flatten.

TABLE III. Binding energies of selected standard dimer pattern structures (see Figs. 2 and 6).

Sr coverage (ML)	Pattern	Fig.	E_{bind} (eV)/Sr
Isolated	A site	2, top	3.64
Isolated	D site	2, bottom	3.23
Isolated at step edge	D_B [a]		3.75
1/6	Single chain	6(a)	3.82
1/4	Double chain	6(b)	3.78
1/2	All A site	6(c)	3.54
1/2	AAAD	6(d)	3.50
1/2	Single D, remainder A		3.29

[a]Reference 26.

Due to the importance of double height silicon steps in the experiments of Reiner *et al.*[7] (see Sec. III), we also considered the binding of a Sr atom to a double height silicon step (D_B in Chadi's notation[26]) which we found to be 3.75 eV. While this binding energy is larger than the binding of an isolated Sr atom to the dimerized surface, it is smaller than the most stable 1/6 ML chain structures presented below (see Table III); therefore, we do not expect Sr atoms to bind preferentially to step edges nor step edges to necessarily be important sites of nucleation for the observed changes in surface structures.

Following Ashman *et al.*,[9] we began to search the phase space for higher coverages of Sr on the surface. We found that the most stable structures were those where the surface silicon atoms were able to arrange their buckling such that as many raised surface silicon atoms were nearest neighbors of the Sr as possible, without the Sr aggregating into locally high coverage patches. This condition is generally met by diagonal chains of Sr atoms, which allow the Sr atoms in adjacent rows to be linked by flattened dimers and also allow the remaining buckled dimers near the Sr to arrange their buckling to both keep raised Si atoms near the Sr and maintain an alternately buckled pattern in each row.

For example, at 1/6 ML, we found the most stable structure to be chainlike patterns of Sr atoms occupying the A site [see Fig. 6(a) and Table III]. This structure has a very strong binding energy of 3.81 eV/Sr. It is important to note that while in principle this structure will be ordered at zero temperature, there exist zigzag chain structures which are essentially isoenergetic with the straight chains. In fact, we found that the zigzag chains are 0.014 eV/Sr more stable than the straight chains at 1/6 ML. This energy difference is essentially within our convergence threshold and likely beyond the accuracy of the PBE GGA functional, but were it accurate, we would expect the chains to be disordered well below room temperature. This near degeneracy between straight and kinked chains causes the positions of Sr atoms in second-nearest-neighbor rows in the $2\times$ direction to be very weakly correlated; therefore, we expect the Sr pattern for this reconstruction to appear disordered, in contrast to the ordered 2×3 reconstruction observed at 600 °C in RHEED experiments (Table II).

As we increased the Sr coverage, the next coherent phase on silicon dimer rows was the double chain structure at 1/4 ML [see Fig. 6(b) and Table III]. This structure is similar to the single chain structure, but with each chain having two consecutive A sites filled, which again maximizes the number of raised dimer atoms near each a surface Sr. For the same reasons as the single chain, this structure will also be disordered at finite temperatures.

Finally, at 1/2 ML Sr coverage, we found the most stable structure to have every A site filled, which produces a coherent 2×1 diffraction pattern [see Fig. 6(c) and Table III]. If each Sr atom fully donated two valence electrons to the silicon surface, this structure would have every Si dangling bond passivated, and we did find that the surface has a band gap (see Fig. 4). However, our Wannier function calculations indicated that the bonding is more covalent than previously thought, as there was significant hybridization between the Si dangling bonds and the Sr orbitals [see Figs. 3(a)–3(c)]. This

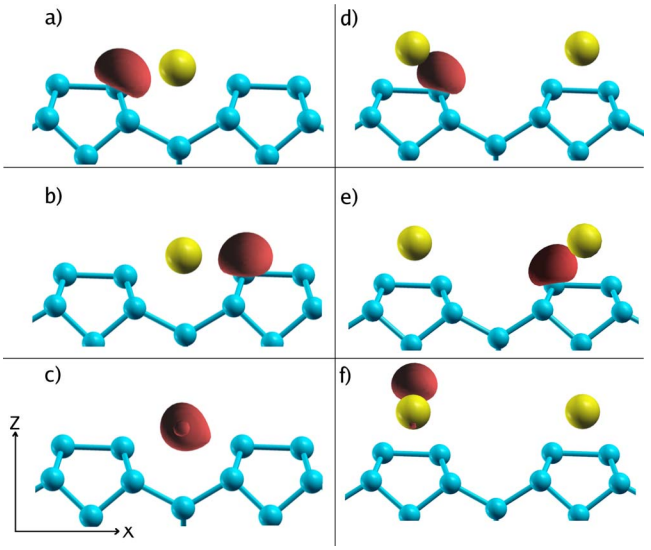

FIG. 3. (Color online) Isosurface plots of bonding state Wannier functions at 1/2 ML coverage (red regions are positive). (a) and (b) A site Si dangling bonds. (c) A site low-energy Sr state. (d) and (e) D site Si dangling bonds. (f) D site low-energy Sr state. Note that the Sr states in (c) and (f) are centered between the Sr atoms along the *y* direction, perpendicular to the plane of the figure.

strong overlap between Si and Sr states pushes the Sr states out of the silicon band gap. We can understand this process better by examining the Wannier functions for the D site 2 $\times$1 ML structure. By comparing Figs. 3(a)–3(c) with Figs. 3(d)–3(f), we can see that while the silicon states are very similar, the lowest energy Sr state for the D structure is much farther from the surface and has much less overlap with the dangling bonds than in the A site case. This difference results in Sr states interacting less with the silicon and remaining in the middle of the silicon band gap (compare Figs. 4 and 5), which accounts for the large difference in binding energies between the A site and D site (Table III). Additionally, in

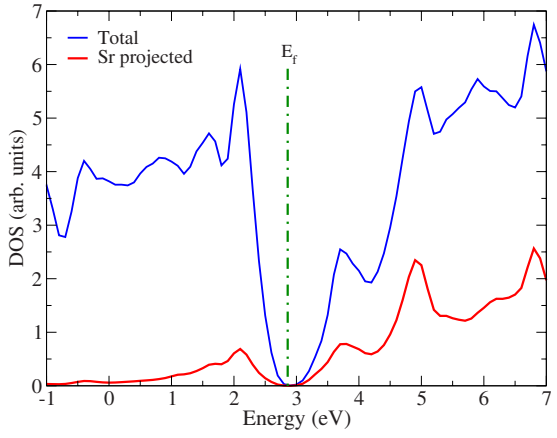

FIG. 4. (Color online) Total density of states (DOS) in blue (upper curve) and Sr projected DOS from sp^3 Wannier function calculations in red (lower curve) for the 1/2 ML all A site structure. The strong interaction between the Sr states and Si states [see Figs. 3(a) and 3(b)] pushes the Sr levels away from the Fermi level (vertical dashed), opening a band gap.

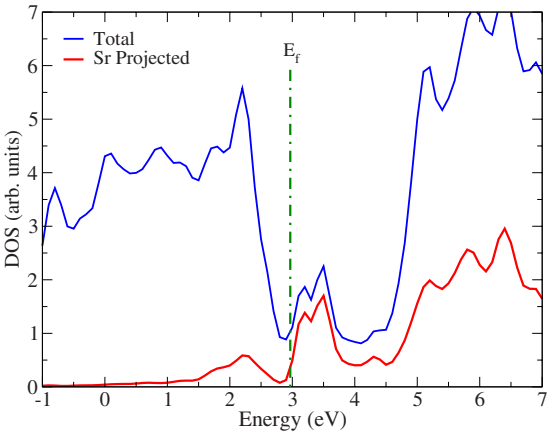

FIG. 5. (Color online) Total DOS in blue (upper curve) and Sr projected DOS from sp^3 Wannier function calculations in red (lower curve) for the 1/2 ML all D site structure. The weaker interaction between the Sr states and Si states [see Figs. 3(c) and 3(d)] results in Sr levels in the silicon band gap and less hybridization between Sr states and Si states. The Fermi level is the vertical dashed line.

both cases, there is a significant contribution to the density of states below the Fermi level which has Sr character. A pure ionic model would have no occupied Sr valence states. Thus, these contributions indicate a hybridization between the silicon dangling bonds and the Sr orbitals in a covalent bonding picture. By comparing our Wannier function calculations with and without Sr *d* orbitals, we found that both Sr *s* and *d* orbitals contribute to this bonding.

Because of the importance of the 1/2 ML A site structure in epitaxial oxide growth and interface formation, we were interested in determining how disordered it might become at finite temperatures. Namely, we wanted to know the lowest energy localized excitations of this surface. Due to the ordered Sr pattern, with all of the A sites filled, as well as the highly directional nature of silicon sp^3 bonding, the only available low-energy surface excitation is to move a single Sr atom from an A site to a D site. In order to calculate this energy, we compared the energy of a 4$\times$4 patch of the 1/2 ML all A site structure to the same 4$\times$4 patch except with a single A site Sr atom moved to a neighboring D site. We found that this excitation requires 0.25 eV of energy. While this D site excitation energy is much less than the 0.60 eV/Sr required to move all of the A sites to D sites at 1/2 ML coverage, it is still several times k_bT (0.075 eV at 600 °C, a typical deposition temperature). If we make the simple approximation that each Sr atom on the 1/2 ML surface can occupy either an A site or a D site and is uncorrelated with the other Sr atoms, we find that less than 4% of the Sr will be in D sites. While calculations with a higher density of defects (e.g., AAAD in Fig. 6 and Table III) indicate that there is an attraction between second-nearest-neighbor D sites which partially stabilizes higher densities of D sites, due to the low density of defects at deposition temperatures, these interactions will not occur frequently enough to change our simple estimate significantly.

The 2$\times$1 all A site structure is consistent with the low temperature RHEED results and is the most stable structure

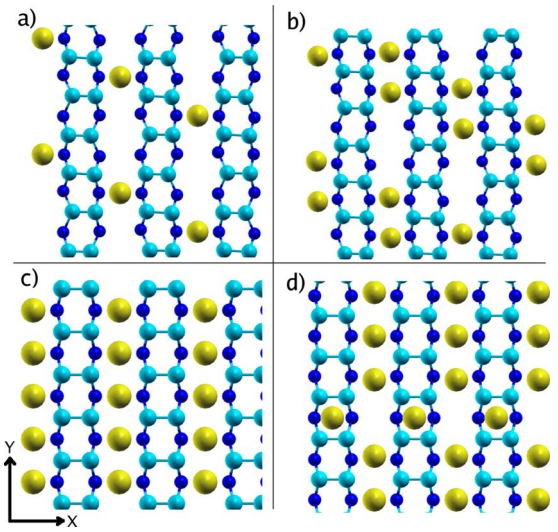

FIG. 6. (Color online) Top view of (a) 1/6 ML chain, (b) 1/4 ML double chain, (c) 1/2 ML all A site, and (d) 1/2 ML AAAD structure. Sr are the largest atoms and are in yellow, the silicon dimers are medium sized and in light blue, and the second level Si atoms are smallest and in dark blue.

at 1/2 ML coverage we found in our work. However, while this 2×1 pattern has the correct size unit cell, it cannot by itself explain the 1×2 pattern seen at high temperatures because the 1×2 pattern is perpendicular to the original dimers (see Table II). The only reasonable way the surface dimers can change orientation is for an entire layer of silicon to leave the surface, exposing the second layer of silicon atoms, which then naturally reconstructs into perpendicular dimers. Unfortunately, standard dimerized surface silicon structures provide no thermodynamic driving force for the 2×1 to 1×2 transition: the starting point and ending point have identical free energies by rotational symmetry. This lack of driving force, together with the failure to explain the observed 2×3 pattern at 1/6 ML, forces us to rule out this entire class of structures when attempting to explain the high temperature growth experiments.

V. MODIFIED DIMER PATTERNS

When the silicon surface was constrained to be in the original dimer pattern (Sec. IV), the calculated reconstruction patterns could not explain the observed high temperature surface symmetries of Table II. In this section, we detail how we considered and then ruled out the possibility that the experimentally observed 2×3 and 1×2 symmetries could be due to the influence of configurational or vibrational entropy on a stoichiometric silicon surface. (This ruling out was necessary to justify the explanation of the experimental data presented in Sec. VII. As we show below in this section, none of the structures we found in this class were thermodynamically stable under growth conditions when compared to those of Sec. IV.)

We began by searching modified dimer patterns that have similar local silicon bonding to the standard dimerized silicon surface but allow greater numbers of Sr configurations.

TABLE IV. Binding energies of selected modified dimer pattern structures (see Fig. 7). All modified dimer patterns are less energetically favorable than the lowest energy 2×1 dimer reconstructions at the corresponding Sr coverages (see Table III); however, they can be stabilized by entropic effects at high temperatures.

Si pattern	Sr coverage (ML)	Sr pattern	Fig.	E_{bind} (eV)/Sr
2×1	1/2	A site	6(c)	3.53
$c(2\times2)$	1/2	$c(2\times2)$	7(a)	3.45
$c(2\times2)$	1/2	Rows	7(b)	3.44
$c(2\times2)$	1/2	Columns		3.02
$c(2\times4)$	1/2	Rows	7(c)	3.48
$c(2\times4)$	1/2	$c(2\times4)$	7(d)	3.41
$c(2\times6)$	1/2	AAA		3.45
$c(2\times6)$	1/3	Rows		3.51
$c(2\times6)$	1/3	AA		3.43
2×3	1/2	AAA_{shift}		3.42
2×3	1/2	Row+A		3.41

These patterns consist of Sr atoms adsorbed on Si surfaces where all surface Si form dimers, but the dimers themselves are not arranged into rows (see Fig. 7 for some examples). For bare silicon surfaces, these silicon patterns are all unfavorable when compared to the normal 2×1 pattern, but only by about 0.06 eV/1×1 surface area, which is small compared to typical Sr binding energies and on the order of k_BT at typical deposition temperatures (see Table IV and parts of Table V).

We began our search by moving every other silicon dimer out of the row alignment, creating a $c(2\times2)$ silicon reconstruction. When we placed 1/4 ML of Sr on this surface, we found an unfavorable binding energy of 3.37 eV/Sr; however, there were several 1/2 ML structures with binding energies which were nearly competitive with the previously considered 2×1 all A site structure (see Table IV and Fig. 6).

While these $c(2\times2)$ silicon structures are less stable than the 2×1 all A structure, their geometries allow a greater number of Sr configurations than are possible when the dimers are forced to be in rows and only A sites are occupied. For instance, some combination of Figs. 7(a) and 7(b) could coexist on the $c(2\times2)$ silicon surface. This configurational entropy should eventually stabilize this structural class relative to the more ordered 2×1 pattern. We made an optimistic estimate of this effect by assuming that each 1×2 surface area had two allowed Sr configurations with energies E_1 and E_2 that were uncorrelated with the other Sr atoms. With these simplifying assumptions, we had the following formula for the configurational free energy:

$$F_{config} = -k_BT \ln\left(\sum_{i=1,2} \exp(-E_i/k_BT)\right). \quad (4)$$

In the limit where $E_1=E_2\approx-3.45$ eV/Sr, we got the simpler formula $F=-3.45$ eV$-k_BT\ln(2)$. This model gives a transition to the $c(2\times2)$ silicon dimer pattern at 1200 °C, which

TABLE V. Surface energies of various bare silicon reconstructions. All surface energies are given per 1×1 silicon area relative to the $p(2\times2)$ buckled dimer row reconstruction. Any submonolayer silicon is assumed to come from a bulk reservoir. All these silicon only structures considered are less stable than the $p(2\times2)$ bulked row reconstruction. The Fig. column refers to figures with the indicated silicon pattern (when Sr is removed).

Si coverage (ML)	Symmetry	Fig.	E_{surf} (eV)/1×1
0	$c(2\times4)$	7(c)	0.07
0	$c(2\times6)$		0.025
0	$c(2\times2)$	7(a)	0.08
0	2×3		0.08
1/3	2×3 DV-2	10(a)	0.09
1/2	2×4 DV-2		0.09
1/2	S_a 2	9(b)	0.03
2/3	S_a 1	9(a)	0.03

is much higher than the temperature where the 1×2 RHEED reconstruction is first observed (Table II).

Using the same techniques, we also investigated several other modified dimer patterns at various coverages, the most stable of which was the $c(2\times4)$ silicon configuration with 1/2 ML of Sr arranged into rows parallel to the dimers [Fig. 7(c)], with a binding energy only 0.05 eV/Sr less favorable than the 2×1 all A structure. However, our simple estimate indicated that the transition to this would be above 1000 °C, again far too high to explain the experiments.

Encouraged by the relatively close energies of these structures, we considered the possibility that the different vibrational modes of these surface structures explained the temperature dependences observed in experiment. While most

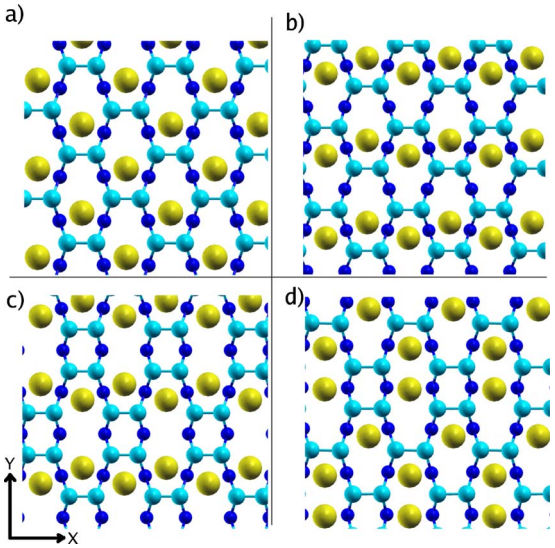

FIG. 7. (Color online) Top view of some low-energy modified dimer pattern reconstructions. (a) $c(2\times2)$ silicon with 1/2 ML Sr in a $c(2\times2)$ pattern; (b) $c(2\times2)$ silicon with 1/2 ML Sr in rows; (c) $c(2\times4)$ silicon with 1/2 ML Sr in rows; and (d) 2×3 pattern with 1/2 ML Sr. Same nomenclature as Fig. 6.

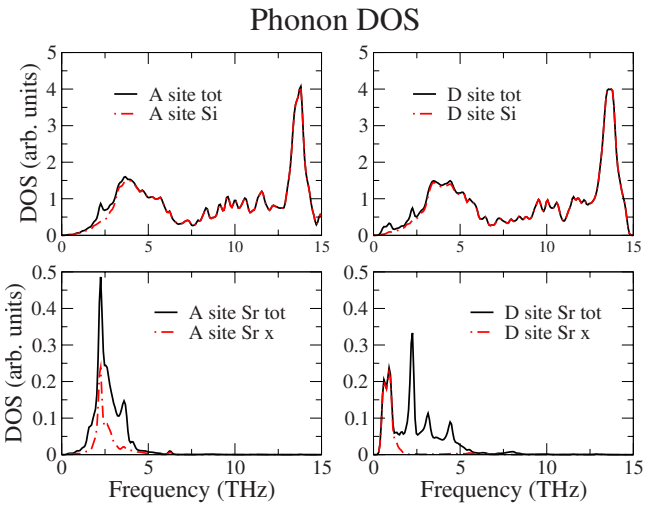

FIG. 8. (Color online) Phonon DOS of 1/2 ML all A and all D site surfaces with 14 layers of silicon. Top: A site (left) and D site (right) total phonon DOS (black solid) and silicon projected DOS (red dashed-dotted). Bottom: A site (left) and D site (right) phonon DOS projected onto all Sr motion (black solid) and Sr x-direction motion, parallel to the dimers (red dashed-dotted). The differences in the frequencies of the Sr x mode account for the majority the difference in the vibrational free energy between the A site and D site (see text).

first-principles calculations assume that the differences in the vibrational free energies of similar structures are negligible, the different bonding geometries combined with the possibility of low frequency modes associated with the relatively heavy Sr atoms created the possibility for strong vibrational effects.

To estimate the size of these vibrational effects, we first calculated the differences in vibrational free energy between the 1/2 ML 2×1 all A site structure and the 1/2 ML 2×1 all D site structure. We found that the contribution from the vibrational free energy favors the D site over the A site (see Fig. 1). The free energy difference between the two structures is primarily due to the low frequency mode corresponding to Sr motion parallel to the dimers (see the lower panels of Fig. 8 in particular). We found that the frequency of this mode is much lower for the D site than for the A site, which can be explained by the fact that D site Sr is sitting above the dimer rows so there is little to prevent it from moving parallel to the dimers. However, despite this low frequency mode, we found that at 600 °C, the difference in vibrational free energy is only 0.057 eV/Sr in favor of the D site which is obviously not enough to offset the 0.60 eV/Sr difference in binding energies between the structures.

Encouraged by the magnitude and sign of this result, we considered the differences in vibrational entropy between the 1/2 ML 2×1 all A structure and the 1/2 ML $c(2\times2)$ structure which should be typical of the bonding scheme in the modified dimer pattern structures. We found that the 2×1 all A structure is further stabilized over the modified dimer pattern by 0.047 eV/Sr at 600 °C due to vibrational effects.

On the basis of these test cases, we concluded that while the differences in vibrational free energy between the 2×1 all A structure and the modified dimer pattern structure are

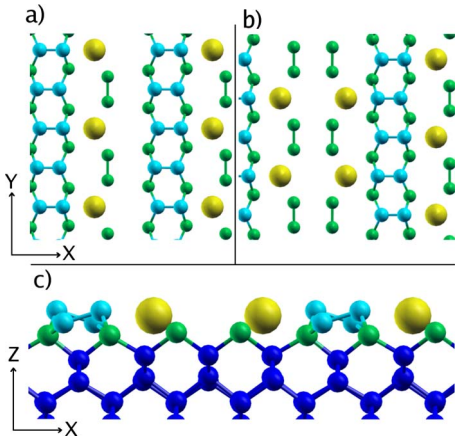

FIG. 9. (Color online) Top and side views of selected S_a structures. (a) Top view of 3×2 1/6 ML structure. (b) Top view of $c(8\times2)$ 1/4 ML structure. (c) Side view of 4×2 or $c(8\times2)$ 1/4 ML structure. The Sr atoms are pictured in yellow, the original silicon dimers (1/3 ML silicon) are in light blue, the second-layer silicon atoms are in green, and lower level silicon are in dark blue.

not entirely negligible compared to their binding energy differences, the effects have the wrong sign to explain the temperature dependent reconstructions observed experimentally. More generally, we expect that even for significantly different structures, the vibrational contributions to the free energy would tend to give a correction of at most 0.05 eV/Sr to the difference in ground state binding energies at typical deposition temperatures.

VI. MOBILE SILICON RECONSTRUCTIONS

After exploring the phase space of Sr atoms sitting on a surface with a full monolayer of silicon, we were still unable to explain the periodicity and the temperature dependence of either the 2×3 or the 1×2 reconstruction observed experimentally. Therefore, we were forced to explore surfaces with submonolayer coverages of silicon.

Structures featuring silicon atoms with less than three Si-Si bonds were quickly ruled out as very unstable as the Sr binding energies tended to be about 2.2 eV/Sr. Additionally, any structures that created more than one Si dangling bond per 1×1 surface area were found to be very unstable. For example, a naive attempt to create a 1/2 ML Sr structure with 1×2 symmetry for the Sr atoms involves removing a column of Si dimers and replacing it with 1/2 ML Sr. However, due to the dangling bonds on the newly exposed second-layer Si, this structure has three dangling bonds per 2×1 area and a correspondingly poor binding energy of 2.95 eV/Sr.

TABLE VI. Sr binding energies of submonolayer silicon S_a structures [see explanation of notation for S_a and other possible steps by Chadi (Ref. 26)]. Sr fill A sites but relative to the second-layer silicon (see Fig. 9).

Si coverage (ML)	Sr coverage (ML)	Pattern	Fig.	E_{bind} (eV)/Sr
2/3	1/6	2×3 A_	9(a)	3.56
2/3	1/3	2×3 AA		3.30
1/2	1/4	$c(2\times8)$ A_A	9(b)	3.58
1/2	1/4	$c(2\times8)$ AA_		3.56
1/2	3/8	$c(2\times8)$ AAA		3.42

TABLE VII. Sr binding energies of submonolayer silicon dimer vacancy structures (see Fig. 10).

Si coverage (ML)	Sr coverage (ML)	Pattern	Fig.	E_{bind} (eV)/Sr
1/3	1/6	$c(2\times6)$	10(a)	3.96
1/3	1/6	2×3	10(b)	3.90
1/3	1/6	4×3		3.80
1/3	1/3	2×3		3.42
1/2	1/8	2×4		3.62

Due to these constraints, we were forced to look for structures where any exposed second-layer silicon atoms were able to reconstruct into subsurface dimers. By searching structures fitting this constraint, we found two relatively stable classes of structures with submonolayer Si coverages. The first class of structures can be thought of as variations in the most stable type of single height steps (denoted as S_a by Chadi[26]). In these structures, rows of dimers are separated by areas of exposed second-layer silicon atoms. The exposed silicon atoms then reconstruct into second-layer dimers, creating a $2\times$ periodicity perpendicular to the original dimers (see Fig. 9). While these structures are surprisingly stable, none of them are more stable than the standard dimer row structures at the same coverage, and furthermore, they quickly become unfavorable at coverages approaching 1/2 ML (compare Tables III and VI). Hence, we excluded these structures from further consideration.

The second structure class, on the other hand, features several structures that are more thermodynamically stable than any of those we or others considered previously. These structures are created by removing two adjacent dimers in a row (i.e., removing two dimers along the original $1\times$ or y direction), reconstructing the exposed silicon atoms into new dimers perpendicular to the original dimers, and placing a Sr atom in the created hole (see Fig. 10). (These structures are similar to the DV-2 dimer vacancy defect studied by Wang *et al.*[28]) In particular, both the 2×3 and $c(2\times6)$ 1/6 ML dimer vacancy reconstructions are more stable than the single chain 1/6 ML reconstruction previously considered as the most favorable (compare Tables III and VII). The energy differences of 0.1 eV/Sr or more between these structures and the single chain at 1/6 ML are larger than any likely difference in vibrational free energy at deposition temperatures.

In order to understand the unusual stability of these structures, we explored the electronic density of states of these structures and were surprised to find that these 1/6 ML surfaces are insulating (see Fig. 12). This is despite the fact that in the limit of pure ionic Sr-Si electron transfer, there are six dangling Si orbitals with only eight electrons to fill them (see Fig. 13 before interaction). In order to understand this behav-

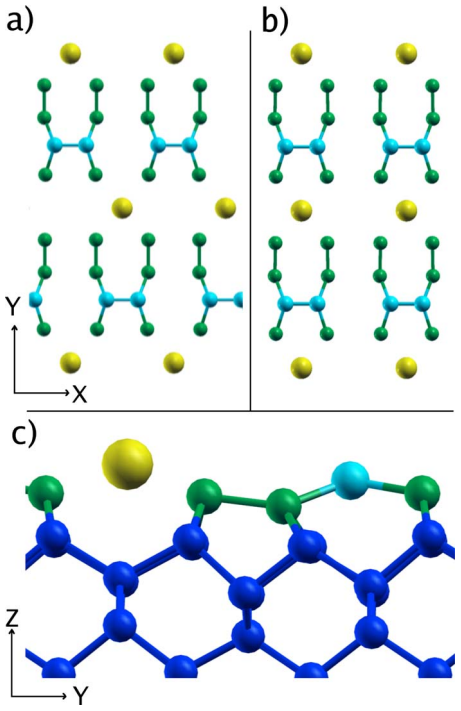

FIG. 10. (Color online) Top view and side view of selected dimer vacancy structures. (a) Top view of $c(2\times6)$ 1/6 ML structure. (b) Top view of 2×3 1/6 ML structure. (c) Side view of 2×3 or $c(2\times6)$ 1/6 ML structure. The Sr atom is large and yellow, the original silicon dimer (1/3 ML silicon) is in light blue, the second-layer silicon atoms are in green, and lower level silicon are in dark blue.

ior, we employed maximally localized Wannier functions to project the contributions of various orbitals to the density of states. In all of our Wannier function calculations, we used *s* and *d* Sr states. To obtain a qualitative understanding of the surface, we only added the surface silicon states. For a more quantitative understanding of the band structure and density of states, we added an sp^3 basis for the surface and subsurface silicon in our calculations.

We found that the Sr *s* and *d* states [Fig. 11(D)] interact strongly with the orbitals belonging to the four Si atoms surrounding the Sr atom [Figs. 11(A) and 11(B)]. This interaction pushes these Sr states much higher in energy and so these Sr-derived states donate their electrons to the Si-derived orbitals (note the red curve in Fig. 12 that shows some hybridization below the Fermi level). Figure 13 shows a schematic explanation of the energy levels and Fig. 12 displays the density of states.

More surprisingly, we found that the dangling bond states on the original surface dimer were rather high-energy unoccupied states with strong p_z character [Fig. 11(C)]. This effect is due to a significant flattening of the original dimer: the dimer unbuckles and both atoms move closer to the surface due to the stretching of neighboring bonds. This results in a planar sp^2-like bonding scheme with a high-energy dangling p_z-like state. These p_z-like states also donate their electrons to the second-layer Si dangling orbitals, causing a band gap to open (see the dotted magenta line in Fig. 12, as well as the schematic picture in Fig. 13). The band gap is widened by

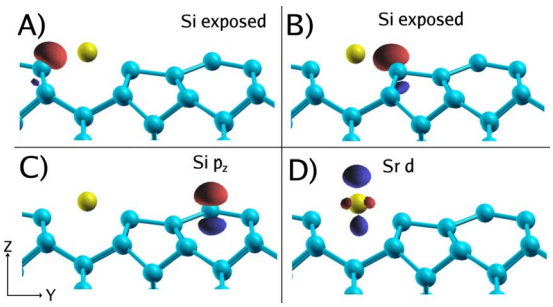

FIG. 11. (Color online) Side view of 2×3 1/6 ML dimer vacancy structure with Wannier functions of selected surface states when using the minimal basis for the Si surface. Red and blue lobes show positive and negative isosurfaces of the Wannier functions. (A) and (B) Dangling orbitals of exposed silicon atoms adjacent to the Sr. (C) Unoccupied p_z state on the original surface dimer. (D) One of many unoccupied Sr *d*-character states.

the very strong interaction between the dangling Si states [Fig. 11(A)] and the original dimer states [Fig. 11(C)]. The donation of electrons by the original surface dimer, as well as its interaction with the surrounding states, account for the unexpected electronic structure.

While these 1/6 ML structures are thermodynamically stable, their formation will be suppressed at low temperatures by the kinetic barrier required to move 2/3 ML of silicon from the surface to step edges, where it can join the bulk silicon. Because silicon adatoms are mobile at typical deposition temperatures,[29] we expected that the energy barrier to break a dimer should provide an order of magnitude estimate for this kinetic barrier. We performed nudged elastic band calculations of a dimer breaking on the surface with various Sr coverages (see Table VIII and Fig. 15). All of our calculations were done in a 2×2 surface cell with the silicon beginning in dimer rows (see Fig. 14). Next, one of the dimer bonds broke as its two silicon atoms move apart. Once the silicon atoms passed the transition state where the bond

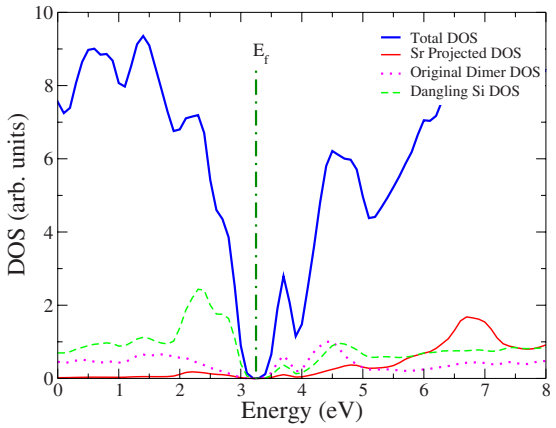

FIG. 12. (Color online) Electronic DOS for the 2×3 1/6 ML Sr structure, projected using Wannier functions with an sp^3 basis for the silicon (see Fig. 13 for a schematic explanation). The upper solid blue line is the total DOS, the lower solid red line is Sr projected DOS [Fig. 11(D)], the dashed green line is exposed silicon projected DOS [Figs. 11(A) and 11(B)], and the dotted magenta line is the original dimer projected DOS [Fig. 11(C)].

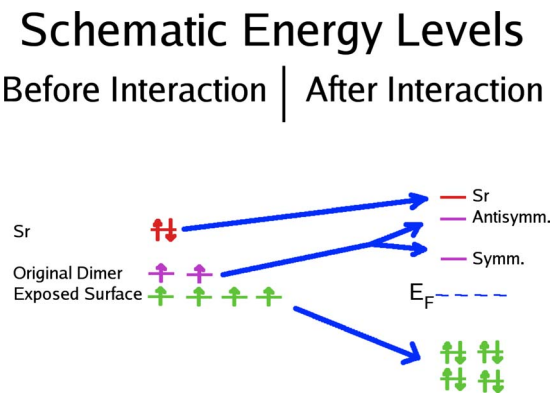

FIG. 13. (Color online) Schematic energy level diagram for 2×3 1/6 ML structure. Strong interactions push the exposed surface silicon levels [Figs. 11(A) and 11(B)] down in energy and the Sr [Fig. 11(D)] and original dimer [Fig. 11(C)] levels up. The original dimer levels also form symmetric and antisymmetric combinations, while the exposed surface atoms interact and form low-energy occupied bands. See Fig. 12, which has matching colors, for the projected DOS and Fig. 11 for real-space plots of the Wannier functions.

was broken, they reformed into a $c(2\times2)$ pattern due to the periodic boundary conditions. We preformed this calculation with no Sr, one Sr in an A site, and two Sr—one in an A site and one in a D site (see Fig. 2). We found that the barriers are large (0.5–1.0 eV) compared to the relevant thermal energy scales and that the barriers were greatly reduced by the presence of Sr (see Table VIII). We attribute this lowering to the electrons from the Sr atom passivating the dangling Si orbitals present in the transition state and thus reducing its energy.

By using simple transition state theory, we could make an estimate of the rate of dimer breaking, which was our rate limiting step (see Table VIII). Our estimate for the prefactor for our transition state theory calculations was 4×10^{12} Hz, which we calculated to be a typical frequency of a dimer vibrating in the x direction.

By comparing these rates to an average experimental deposition time of 1 min, we could determine whether the silicon was mobile at any given temperature. According to the rates in Table VIII, we expect that the surface silicon should be frozen for room temperature deposition but highly mobile at 600 °C. Also, by looking at the variation in energy barriers with coverage, we find that submonolayer coverages of Sr on Si strongly encourage the motion of silicon on the surface (see Fig. 15).

TABLE VIII. Nudged elastic band and simple transition state theory results. We calculated the energy barrier to break a silicon dimer and used simple transition state theory to estimate the rate at both low and high deposition temperatures (see Fig. 14).

Sr coverage (ML)	$E_{barrier}$ (eV)	Rate at 0 °C (Hz)	Rate at 600 °C (Hz)
0	1.29	7×10^{-12}	2×10^{5}
1/4	0.92	5×10^{-5}	2×10^{7}
1/2	0.63	1×10^{2}	1×10^{9}

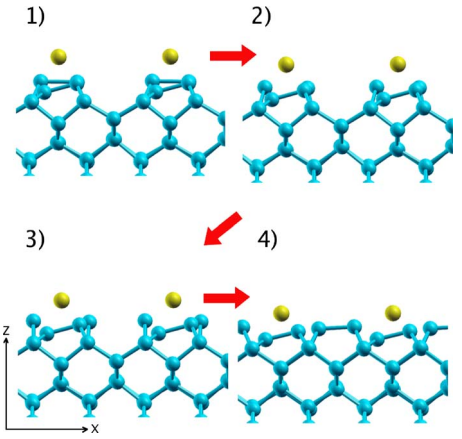

FIG. 14. (Color online) Transition from silicon 2×1 dimer pattern to $c(2\times2)$ pattern with 1/4 ML Sr on surface. The silicon begins in a 2×1 dimer pattern, which is a local minimum in (1). The dimer breaks in (2) and continues to the transition state in (3). Due to periodic boundary conditions, the dimer then reforms in (4) in the $c(2\times2)$ pattern, another local minimum. On a real surface, the now separate silicon adatoms would be able to diffuse freely after (3). The energy barrier for this process is 0.92 eV.

VII. EXPLANATION OF EXPERIMENTAL GROWTH

With the addition of the results on mobile silicon surfaces (Sec. VI), we can now understand and explain the symmetries observed during Sr deposition under both high temperature and low temperature conditions. Figure 16 shows a schematic that organizes the discussion. Both high and low temperature depositions begin with a 2×1 dimer pattern on the bare silicon surface. At low temperatures, in accordance with our dimer breaking rate results, this dimer pattern is frozen in place and the Sr sit on top of the dimerized surface and settle into A sites. We expect these A sites to arrange themselves locally into the single chain structure at 1/6 ML and the double chain structure at 1/4 ML. However, both of these patterns will be disordered, explaining the lack of a coherent diffraction pattern at these coverages. When the Sr coverage reaches 1/2 ML, all the A sites will be filled, and the surface will display a 2×1 reconstruction consistent with experiment.

On the other hand, when the deposition is conducted at high temperature, the surface will not be frozen into a dimer pattern. In particular, as a coverage of 1/6 ML of Sr is approached, we expect the surface to transition into one of the low-energy dimer vacancy patterns with 2/3 of the silicon dimers moving to step edges (see Fig. 16). While our lowest energy 1/6 ML structure has a $c(2\times6)$ reconstruction, the very similar 2×3 reconstruction is only 0.06 eV/Sr less stable (see Table VII) and matches the experimental observations.[7,25] We speculate that the 2×3 structure is stabilized experimentally due to step edge effects, as the step edges appear straight in STM images,[25] which is incompatible with a $c(2\times6)$ reconstruction. These step edge effects will be especially large for the 4° miscut silicon wafers used in RHEED experiments[7] since these wafers have terraces that are only ten silicon (001) unit cells wide.

As Sr coverage is further increased at high temperatures, the extra Sr will begin to form patches of the 1/4 ML double

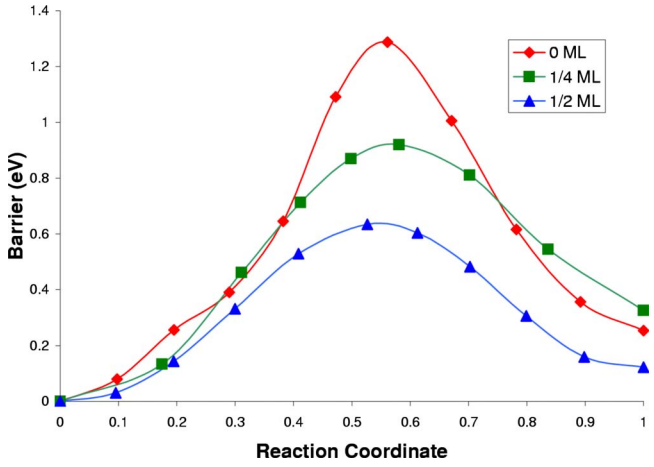

FIG. 15. (Color online) Energy barrier versus reaction coordinate for nudged elastic band calculations of dimer breaking (see Fig. 14 and Table VIII). Red diamonds are for the bare silicon surface, green squares are for 1/4 ML Sr on surface, and blue triangles are for 1/2 ML Sr. The lines are guides for the eyes. The reaction coordinate goes from 0, where the dimer is in its equilibrium position, through the transition state near 0.5 and continues to 1, where the dimer atoms recombine with periodic copies into a metastable modified dimer row structure.

chain reconstruction [see Figs. 6(b) and 16]. As these patches of 1/4 ML dimerized surface grow, the remaining 1/3 ML of silicon must also move to step edges. When this process is complete, one full monolayer of silicon has been removed from the surface, and the dimers will now be oriented perpendicular to the original surface dimers, accounting for the observed 1×2 surface symmetry. As more Sr is deposited, from 1/4 to 1/2 ML, the double chain patches will change continuously into 1/2 ML all A site patches. Therefore, the high temperature 1/2 ML reconstruction will have the same atomic structure as the low temperature 1/2 ML reconstruction but rotated 90° with respect to the original dimers. The rotation simply reflects the geometry of bulk Si: atoms in successive (001) planes have identical surroundings except for a 90° rotation around [001].

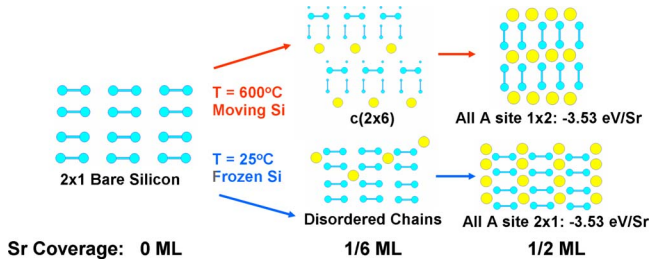

FIG. 16. (Color online) Schematic phase diagram of submonolayer Sr on Si(001). Each diagram shows a top view of the surface with silicon surface atoms and dimers in light blue and the larger Sr in yellow. Both the low and high temperature systems begin with a 2×1 dimerized bare silicon surface, but as Sr coverage increases they follow different paths. At 600 °C, the silicon is free to move on the surface, and the surface remains in thermodynamic equilibrium. However, at 25 °C, silicon motion is prevented by a kinetic barrier, and the lowest energy dimerized surface structure is formed.

Since the low and high temperature reconstructions are identical up to a rotation, it should be possible to grow an oxide on both surfaces equally well. In order to investigate this possibility, our colleagues grew BaO on both the high temperature 1×2 and low temperature 2×1 1/2 ML Sr template layers.[7] As expected, both template layers promoted excellent epitaxy between the Si and BaO. This experimentally demonstrates that the 2×1 and 1×2 1/2 ML Sr surfaces are physically identical. Furthermore, a sample grown at an intermediate temperature which displayed an incomplete transition to the 2×3 pattern displayed poor epitaxy. We believe that this is caused by the intermediate temperature template layer failing to change completely from a 2×1 to a 1×2 dimer pattern, which prevents large scale epitaxy. These experiments both confirm our calculations and demonstrate a previously unknown low temperature path to silicon epitaxy.

VIII. SIMULATED STM

A recent paper by Du *et al.*[25] features high resolution scanning tunneling microscopy images of the 2×3 1/6 ML Sr on Si(001) surface as well as a proposal for its atomic structure based on DFT calculations. We considered that proposed theoretical structure and we found that its binding energy was 1.93 eV/Sr, which is considerably less stable than any of the 1/6 ML structures considered in this work (compare to Table VII). We also computed simulated STM images using the method of Tersoff and Hamann[30,31] to compare with the experimental images. We found very good agreement between our low-energy 2×3 dimer vacancy structure (Table VII and Fig. 10) and the experimental STM images.

In agreement with experiment, our filled state image [Fig. 17(a)] had a single large protrusion, which corresponded to the four filled Si dangling bonds surrounding the Sr atom, which were too close together to be resolved experimentally.

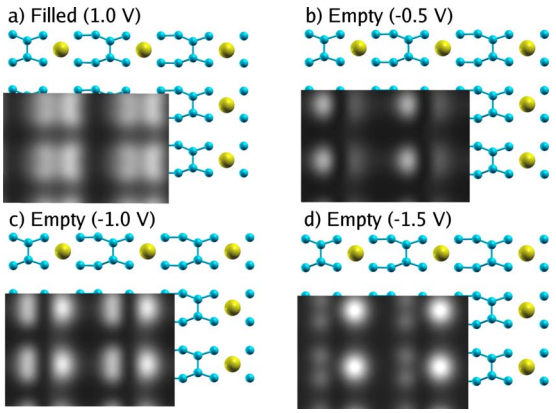

FIG. 17. (Color online) Simulated STM images of the 2×3 dimer vacancy structure (Fig. 10) overlayed on atomic coordinates. (a) Filled states at 1.0 V bias. (b)–(d) Empty states at −0.5, −1.0, and −1.5 V, respectively. The images show the local density of states integrated from the Fermi level to the desired voltage at a constant height of about 5 Å above the surface. The scale runs linearly from zero intensity (black) to the maximum value at the chosen height (white).

Wannier function plots of these states can be seen in Figs. 11(A) and 11(B). Also in agreement with Du *et al.*,[25] the shape of this protrusion depended only weakly on the applied tip-sample bias.

In contrast to the filled state image, but also in agreement with experiment, our empty state images [see Figs. 17(b)–17(d)] had two protrusions. One of these protrusions corresponded to the empty p_z orbitals on the original dimer, which are depicted in Fig. 11(C). The other protrusion corresponded to the empty Sr *s* and *d* states, one of which is shown in Fig. 11(D). The relative size and shape of these two protrusions depended sensitively on the applied bias [compare Figs. 17(b)–17(d)]. This behavior can be understood by looking at the projected electronic density of states (Fig. 12). At low bias (0.5 V in our theory and 1.0 V in experiment), the image is dominated by the empty p_z orbitals, which form the majority of the bottom of the conduction band (see Fig. 12). However, at higher bias, the image is dominated by the Sr orbitals, which are higher in energy and extend further from the surface than the p_z orbitals. Additionally, the protrusion corresponding to the empty Sr states changes shape from elliptical at low bias to circular at high bias [compare Figs. 17(b) and 17(d)]. Both this change in brightness and the change in shape agree with the experimental images of Du *et al.*[25] All qualitative features of the calculated STM images, including the image shapes and bias dependence, agree with the experimental images, which provide further proof that our 1/6 ML 2×3 dimer vacancy structure is the experimentally observed structure.

Quantitatively, the change in ellipticity in the images happens at approximately 0.5 V lower bias in our theoretical calculations than in the experimental images. We attribute this fact to the well-known underestimation of the band gap in DFT calculations. In our calculation, the band gap of silicon is only 0.6 eV, as compared to the experimental value of 1.2 eV. We believe that this is the reason for the $\approx$0.5 V offset in conduction band features between theory and experiment.

IX. CONCLUSIONS

We have presented the surface reconstructions of submonolayer coverages of Sr on Si(001) at both low and high deposition temperatures. Our findings explain the previously unknown 2×3 reconstruction observed experimentally at high temperature and 1/6 ML Sr coverage. This structure, which agrees with both RHEED and STM data, is a key to understanding the effects of temperature on the 1/2 ML phase, which is important in epitaxial oxide growth. At low temperatures, this 1/2 ML phase is created by filling Sr into spaces between the dimer rows, which remain intact. At high temperatures, the formation of the 2×3 phase at 1/6 ML Sr coverage disrupts the original dimer pattern and forces the motion of 2/3 of the surface Si to step edges. The deposition of additional Sr causes the rest of the original surface Si layer to move to the step edges and a dimer pattern to reform on the now exposed second silicon layer. This new dimer pattern is rotated 90° relative to the original dimers since an entire monolayer of silicon has moved.

Understanding this process has clarified the role of temperature in the deposition of epitaxial oxides on Si(001) and has predicted an experimentally verified low temperature path to oxide epitaxy on Si. Further work must be done to compare the quality of the interfaces achieved via the low temperature and high temperature deposition paths. Furthermore, understanding the reconstructions of Sr on Si at the atomic level helps explain the role of Sr in promoting oxide epitaxy on Si and provides important information for future work on oxide epitaxy on Si.

ACKNOWLEDGMENTS

We wish to acknowledge many helpful discussions with our colleagues J. W. Reiner, F. J. Walker, and C. H. Ahn. This work has been supported by the National Science Foundation under Grant No. MRSEC DMR 0520495. Computational resources were provided by Yale High Performance Computing.

*kevin.garrity@yale.edu

[1] International Technology Roadmap for Semiconductors, 2007, http://www.itrs.net
[2] G. D. Wilk, R. M. Wallace, and J. M. Anthony, J. Appl. Phys. **89**, 5243 (2001).
[3] J. Robertson, Rep. Prog. Phys. **69**, 327 (2006).
[4] R. A. McKee, F. J. Walker, and M. F. Chisholm, Phys. Rev. Lett. **81**, 3014 (1998).
[5] R. A. McKee, F. J. Walker, M. B. Nardelli, W. A. Shelton, and G. M. Stocks, Science **300**, 1726 (2003).
[6] C. J. Först, C. R. Ashman, K. Schwarz, and P. E. Blöchl, Nature (London) **427**, 53 (2004).
[7] J. W. Reiner, K. F. Garrity, F. J. Walker, S. Ismail-Beigi, and C. H. Ahn, Phys. Rev. Lett. **101**, 105503 (2008).
[8] D. O. Klenov, D. G. Schlom, H. Li, and S. Stemmer, Jpn. J. Appl. Phys., Part 2 **44**, L617 (2005).
[9] C. R. Ashman, C. J. Först, K. Schwarz, and P. E. Blöchl, Phys. Rev. B **69**, 075309 (2004).
[10] P. Hohenberg and W. Kohn, Phys. Rev. **136**, B864 (1964).
[11] W. Kohn and L. Sham, Phys. Rev. **140**, A1133 (1965).
[12] J. P. Perdew, K. Burke, and M. Ernzerhof, Phys. Rev. Lett. **77**, 3865 (1996).
[13] N. Troullier and J. L. Martins, Phys. Rev. B **43**, 1993 (1991).
[14] A. A. Stekolnikov, K. Seino, F. Bechstedt, S. Wippermann, W. G. Schmidt, A. Calzolari, and M. Buongiorno Nardelli, Phys. Rev. Lett. **98**, 026105 (2007).
[15] S. Baroni, P. Giannozzi, and A. Testa, Phys. Rev. Lett. **58**, 1861 (1987).
[16] P. Giannozzi, S. de Gironcoli, P. Pavone, and S. Baroni, Phys. Rev. B **43**, 7231 (1991).
[17] S. de Gironcoli, Phys. Rev. B **51**, 6773 (1995).
[18] N. Mounet and N. Marzari, Phys. Rev. B **71**, 205214 (2005).

[19] H. Jonsson, G. Mills, and K. W. Jacobsen, in *Classical and Quantum Dynamics in Condensed Phase Simulations*, edited by B. J. Berne, G. Ciccotti, and D. F. Coker (World Scientific, Singapore, 1998), p. 385.
[20] G. Henkelman, B. P. Uberuaga, and H. Jónsson, J. Chem. Phys. **113**, 9901 (2000).
[21] A. A. Mostofi, J. R. Yates, Y.-S. Lee, I. Souza, D. Vanderbilt, and N. Marzari, Comput. Phys. Commun. **178**, 685 (2008).
[22] J. Lettieri, J. H. Haeni, and D. G. Schlom, J. Vac. Sci. Technol. A **20**, 1332 (2002).
[23] W. C. Fan, N. J. Wu, and A. Ignatiev, Phys. Rev. B **42**, 1254 (1990).
[24] R. Z. Bakhtizin, J. Kishimoto, T. Hashizume, and T. Sakurai, J. Vac. Sci. Technol. B **14**, 1000 (1996).
[25] W. Du, B. Wang, L. Xu, Z. Hu, X. Cui, B. C. Pan, J. Yang, and J. G. Hou, J. Phys. Chem. **129**, 164707 (2008).
[26] D. J. Chadi, Phys. Rev. Lett. **59**, 1691 (1987).
[27] A. Ramstad, G. Brocks, and P. J. Kelly, Phys. Rev. B **51**, 14504 (1995).
[28] J. Wang, T. A. Arias, and J. D. Joannopoulos, Phys. Rev. B **47**, 10497 (1993).
[29] A. P. Smith and H. Jónsson, Phys. Rev. Lett. **77**, 1326 (1996).
[30] J. Tersoff and D. R. Hamann, Phys. Rev. Lett. **50**, 1998 (1983).
[31] J. Tersoff and D. R. Hamann, Phys. Rev. B **31**, 805 (1985).